

Experimental and theoretical study of S 2p and C 1s generalized oscillator strengths in CS₂

C.C. Turci^{a,*}, A.B. Rocha^a, M. Barbatti^a, C.E. Bielschowsky^a, I.G. Eustatiu^b,
T. Tyliszczak^{c,1}, G. Cooper^c, A.P. Hitchcock^c

^a Instituto de Química, Univ. Fed. do Rio de Janeiro, Rio de Janeiro, RJ 21949-900, Brazil

^b Department of Physics and Astronomy, McMaster University, Ont. L8S 4M1, Canada

^c Department of Chemistry, McMaster University, Hamilton, Ont. L8S 4M1, Canada

Available online 8 December 2006

Abstract

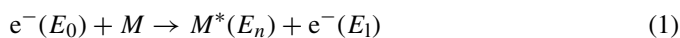
The generalized oscillator strength profiles in the momentum transfer range (K) of ($2 \text{ a.u.}^{-2} < K^2 < 30 \text{ a.u.}^{-2}$) for the most intense resolved S 2p, and C 1s transitions of carbon disulfide (CS₂) are presented. Optical oscillator strengths and generalized oscillator strength profiles have been calculated for vertical excitation from the ground $X^1\Sigma_g^+$ electronic state to several C(1s) and S(2p) inner-shell electronic excited states of CS₂, using high level *ab initio* (HF-CI) calculations. The experimental and computed GOS profiles of CS₂ are compared and found to be generally in reasonable agreement.

© 2006 Elsevier B.V. All rights reserved.

Keywords: CS₂; Generalized oscillator strengths; Inner-shell excitation; (HF-CI) calculations

1. Introduction

In electron energy loss spectroscopy (EELS), a mono-energetic beam of electrons is elastically and inelastically scattered in single collisions with an atom or molecule in a field free region. The energy and angular distributions of the inelastically scattered electrons give detailed spectroscopic information about the excited states of the target. The basic electron energy loss process can be represented as



where e^- is the colliding electron with incident energy E_0 and residual energy (E_1) after a collision with the target species M that excites a transition from the ground state to an excited state of energy E_n . By energy and momentum conservation, in single scattering conditions $E_n = E_0 - E_1$, where E_n is also the electron energy loss:

$$\underline{K} = \underline{k}_0 - \underline{k}_1 \quad (2a)$$

$$K^2 = |\underline{K}|^2 = |\underline{k}_0 - \underline{k}_1|^2 = k_0^2 + k_1^2 - 2k_0k_1 \cos \theta \quad (2b)$$

where \underline{k}_0 is the wave vector of the incident electron with momentum $|\underline{k}_0|$, \underline{k}_1 the wave vector of the outgoing electron scattered through an angle θ with momentum $|\underline{k}_1|$, and \underline{K} is the resultant momentum transfer. When the incident electron is highly energetic (large E_0) and is scattered through a small angle, the momentum transferred to the target from the colliding electron is very small, the interaction between this electron and the target is weak, and electric dipole processes dominate. When the scattering angle becomes large ($>10^\circ$), the momentum transferred to the target from the incident electron during the collision increases, which results in relaxation of the electric-dipole selection rules.

Electron energy loss spectroscopy (EELS) under variable momentum transfer conditions, provides absolute inelastic cross section information [1,2]. The theoretical framework for the analysis of dipole and non-dipole EELS results within the first Born approximation has been derived by Bethe [3] and elaborated in detail by Inokuti [4]. $f(K)$, the generalized oscillator strength (GOS) for electron scattering [3,4], provides a very useful framework for quantitative analysis of inelastic electron scattering. The momentum transfer dependence of the GOS, called the GOS profile, can help determine the type of transition, thus aiding spectral assignment. In its range of validity (where the first Born approximation holds), the GOS concept condenses the (E_0, θ) variables into a single variable, K^2 (usu-

* Corresponding author.

E-mail address: cassia@iq.ufrj.br (C.C. Turci).

¹ Present address: Advanced Light Source, LBNL, Berkeley, CA 91720, USA.

ally expressed in a.u.⁻²). The GOS is directly proportional to inelastic differential cross section ($d\sigma/d\Omega$) for a transition at a specific energy loss [3,4] given by

$$f(K) = \left(\frac{E_n k_0 K^2}{2k_1} \right) \left(\frac{d\sigma}{d\Omega} \right) \quad (3)$$

For continuum processes the relevant terms are $df(K)/dE$ and $(d^2\sigma/d\Omega dE)$.

This paper presents results of a study of the GOS profiles for C 1s, and S 2p excitation and ionization of CS₂ using a combination of experimental data from electron energy-loss spectroscopy and computational results from *ab initio* configuration interaction and generalized multi-structural calculations. It is part of a systematic determination of GOS profiles for inner-shell transitions [5,6]. The spectroscopic aspects of this study were presented elsewhere [7].

2. Experimental

Electron energy-loss spectra of CS₂ in the regions of C 1s, and S 2p excitations were acquired with a variable impact energy, variable scattering angle ($4^\circ < \theta < 32^\circ$), electron energy-loss spectrometer. The energy resolution was ~ 0.9 eV. A detailed description of the apparatus, its operating procedures and data analysis methods has been published elsewhere [5,6]. Freeze-pump-thaw iterations were performed on CS₂ (stated boiling point range of 46.1–46.6 °C), which was otherwise used as received from the commercial supplier (Aldrich, 99.9% purity). The pressure of the differentially pumped region connected to the gas cell was 5×10^{-6} Torr during data acquisition.

The energy scales of all spectra were calibrated internally using previously published calibrated EELS spectra [8,9]. The procedures used for quantitative analysis of the acquired spectra have been described in detail elsewhere [5,6]. Briefly, the normalized and background subtracted spectra are fit to a combination of Gaussian peak shapes and an error function to represent the ionization continua, using a constrained multi-parameter procedure. Geometric [6] correction is then applied to the peak areas of each feature at each scattering angle to give the cross-section needed to evaluate the relative GOS. The geometrical correction takes into account the angle dependence of the overlap of incident beam, target gas and analyser viewing cone, caused by the change in the size or shape of the interaction region with scattering angle. Relative GOS profiles are then evaluated from the geometry-corrected relative cross sections and the experimentally determined momentum transfer variables, using the Bethe–Born kinematic correction. The relative GOS profiles [5,6] were then placed on an absolute scale by extrapolating relative GOS values to $K^2 = 0$ and then deriving a conversion factor from the match of the relative OOS to the absolute OOS, determined from dipole-regime ISEELS [9].

3. Theory

We have calculated the optical (OOS) and generalized oscillator strength (GOS) for the vertical excitation from the ground

$X^1\Sigma_g^+$ electronic state to several C 1s and S 2p inner-shell electronic excited states of CS₂. The electronic wave functions for the ground and C 1s excited states were determined with the configuration-interaction (CI) method expanded on a C: (12s, 6p, 1d)/[10s, 4p, 1d] and S: (15s, 9p, 1d)/[11s, 5p, 1d] Gaussian basis sets. The employed Gaussian basis sets for the C and S atoms were chosen to achieve a good description of (1) the core molecular orbitals and of (2) the external single occupied orbital after excitation of one electron from the core. Hence, we have used very uncompressed basis sets with several basis functions for the core region and several diffuse functions for the external region.

The molecular geometry has been optimized using the above-described basis set at second-order Møller–Plesset level within $D_{\infty h}$ symmetry; the optimized C–S bond length is 153.8 pm. The occupied and improved virtual orbitals (IVO) were determined independently for the ground and each excited state and, as a consequence, they are not orthogonal. This means that the molecular basis for the CI calculation was optimized for each molecular state and includes, for the excited states, the strong relaxation that takes place in the formation of an inner-shell excited state.

Configuration interaction calculations were performed for each molecular state, allowing single and double excitations (SDCI) for the reference configuration to a virtual space composed of 25 virtual orbitals ($6\sigma_g^+$, $6\pi_g$, $1\sigma_g^-$, $5\sigma_u^+$, $6\pi_u$, $1\sigma_u^-$). In each state, the SDCI calculation was performed for about 6000 configurations.

The second order CI does not balance adequately the fundamental and excited states. This produces errors in the transition energies of about 2 eV. The fourth-order excitations in the CI eliminate these deviations [10]. In our case, computational limitations did not allow to extend the calculation to SDTQ CI level. However, we note that although the absolute values of transition energies were not in good agreement with experimental ones, the relative values show a good agreement [7].

For the excitation from the S 2p orbitals, generalized multi-structural (GMS) wave functions [11,12] were used in order to take into account core hole localization effects without breaking the full molecular symmetry. The GMS wave function is defined as

$$\Psi_{\text{GMS}} = \sum_{l=1}^{N_{\text{STRUCT}}} \sum_{i=1}^{N_{\text{SEF}}} c_i^l \Phi_i^l, \quad (4)$$

where Φ_i^l represents the i^{th} spin-adapted eigenfunction (SEF) of the l^{th} bonding structure and c_i^l its weight in the expansion shown in Eq. (4) and is calculated variationally. Each Φ_i^l is a Hartree–Fock or a CI wave function. We have considered the following three structures ($N_{\text{STRUCT}} = 3$ in Eq. (4)) for each excited state:

- *Structure 1* is a Hartree–Fock wave function with molecular orbitals optimized in the presence of a 2p hole localized upon the first sulphur atom;
- *Structure 2* is a Hartree–Fock wave function with molecular orbitals optimized in the presence of a 2p hole localized upon the second sulphur atom;

- *Structure 3* is a SD CI wave function (SD = single and double) with molecular occupied and virtual orbitals optimized in the presence of a 2p delocalised hole.

This approach considers relaxation, valence correlation and localization effects and retains the full molecular symmetry. The wave functions for the ground (CI) and excited states (CI or GMS), in spite of being a suitable description for the states involved in the transition, have the disadvantage of being mutually non-orthogonal. This requires considerable computational effort for calculating the transition matrix elements. The matrix elements for the scattering amplitude between the non-orthogonal wave functions were calculated using a bi-orthogonalization procedure [13]. For this purpose, unitary transformations are applied to the two sets of N non-orthogonal molecular orbitals, turning $(N-1)$ of them orthogonal.

4. Results and discussion

4.1. Spectroscopy of CS₂

The ground state of carbon disulfide is linear, and can be described by the electron configuration

$$(1\sigma_u)^2(1\sigma_g)^2(2\sigma_g)^2(2\sigma_u)^2(3\sigma_g)^2(3\sigma_u)^2(4\sigma_g)^2(1\pi_u)^4(1\pi_g)^4 \\ \times (5\sigma_g)^2(4\sigma_u)^2(6\sigma_g)^2(5\sigma_u)^2(2\pi_u)^4(2\pi_g)^4(3\pi_u)^*(7\sigma_g)^* \\ \times (6\sigma_u)^*, X^1\Sigma_g^+$$

The lowest energy unoccupied orbitals are $3\pi_u$, $7\sigma_g$ and $6\sigma_u$ which are analogous to the $2\pi_u$, $5\sigma_g$ and $4\sigma_u$ unoccupied orbitals of CO₂ [5].

Fig. 1 presents the C 1s spectra of CS₂ recorded under small ($\theta = 4^\circ$, $K^2 = 1.57 \text{ a.u.}^{-2}$) and large ($\theta = 28^\circ$, $K^2 = 26.6 \text{ a.u.}^{-2}$) momentum transfer conditions. The spectra were obtained with incident electron energy of 1300 eV and are in agreement with the literature (see Table 1) [7,8,14]. The spectra plotted have been normalized to the beam current, gas pressure and acquisition time. A background from extrapolation of the pre-edge signal has been subtracted, but the spectra have not been subjected to the geometric or kinematic corrections. They were calibrated using the energy of 286.1 eV for the C 1s $\rightarrow 3\pi_u^*$ ($^1\Pi_u$) state [15].

At both angles, the spectrum is dominated by the intense feature at 286.1 eV. However there is a dramatic fall-off in intensity as the scattering angle increases - the count rate at 28° is about 250-fold weaker than that at 4° . The dominant peak is the $X^1\Sigma_g^+ \rightarrow ^1\Pi_u$ (C 1s $2\sigma_g^{-1}$, $3\pi_u^*$) transition, analogous to the first discrete peak in the C 1s spectrum of CO₂ [5].

The S 2p spectra of carbon disulfide were also recorded under dipole and non-dipole conditions. The spectra were presented and assignments were discussed in detail elsewhere [7]. For convenience the assignments are also included here to support further discussion of the S 2p spectral assignments in view of the GOS profile results (Table 2).

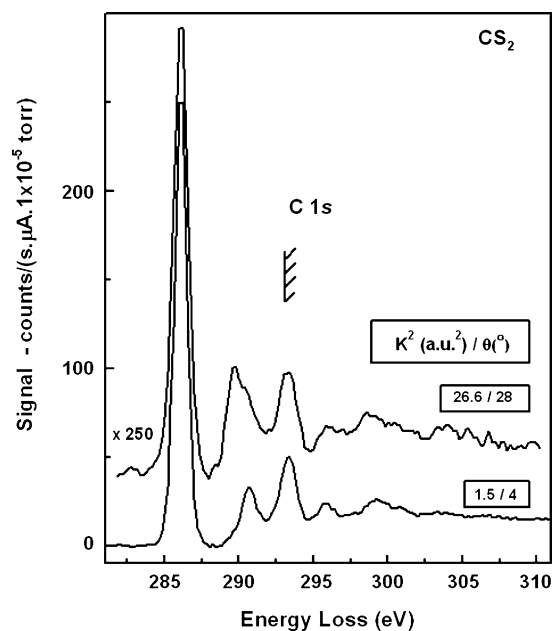


Fig. 1. C 1s electron energy loss spectra of CS₂ recorded with a final electron energy of 1300 eV at 4° ($K^2 = 1.57 \text{ a.u.}^{-2}$) and 28° ($K^2 = 26.6 \text{ a.u.}^{-2}$) scattering angles. The data has been normalized to gas pressure, incident beam current and acquisition time. A background from extrapolation of the pre-edge signal has been subtracted, but the geometric correction has not been applied. Note the 250-fold scale factor between the 4° and 28° data. The hatched line indicates the C 1s IP as determined by X-ray photoelectron spectroscopy [19].

4.2. C 1s generalized oscillator strength profiles

An example of the curve fit used to extract integrated peak areas from the experimental C 1s spectra is presented in Fig. 2. The curve fits at all angles were of similar quality to that displayed in Fig. 2. The GOS profiles for all resolved C 1s spectral features over the K^2 range from 2.0 a.u.⁻² to 30 a.u.⁻² are presented in Fig. 3. The relative GOS profiles were converted to absolute GOS profiles using the optical oscillator strength (OOS)

Table 1

Experimental and computed energies and assignments of C 1s spectral features of CS₂

	Energy (eV)		Assignment	
	Experimental	Theory	Experimental	Theory
1	285.2	286.6 (285.0) ^a	$3\pi_u^*$ ($^3\Pi$)	$[3\pi_u]$
2	286.1	287.7 (286.1)	$3\pi_u^*$ ($^1\Pi$)	$[3\pi_u]$
3	289.4	291.2 (289.6)	$3s\sigma_g^*$ ($^3\Sigma_g$)	$[7\sigma_g]$
4	289.5	291.3 (289.7)	$3s\sigma_g^*$ ($^1\Sigma_g$)	$[7\sigma_g]$
5	290.7	292.3 (290.7)	$3p\sigma_u$	$[6\sigma_u]$
6	292.4	295.4 (290.9)	$3p\pi_u$	$[4\pi_u]$
		296.6 (292.1)	$7\sigma_g^*$ ($^1\Sigma_g$)	$[8\sigma_g]$
		294.1 (292.4)		$[3\pi_g]$
		294.2 (292.6)	IP	
7	293.3	298.0 (293.5)	$6\sigma_u^*$	$[7\sigma_u]$
8	295.8		$2e^-$	
			$2e^-$	
9	299.6		$2e^-$	

^a The values in parentheses are E_{theory} multiplied by a normalization factor f . For the first CI root in each symmetry, f is 286.1/287.7. For the second CI roots, f is 292.1/296.6.

Table 2
Energies and assignments of S 2p spectral features of CS₂

Peak	Energy	Assignment	
	Ref. [7]	2p _{3/2}	2p _{1/2}
1	163.1 ^a	3π _u [*]	
2	164.2		3π _u [*]
3	165.9	7σ _g [*]	
4	166.6	4sσ _g	
5	167.5	4pπ _u /4pσ _u	
6	168.3	3dπ _g /3dδ _g /5sσ _g /5pπ _u /3dδ _g	
7	169.5		5sσ _g /3dδ _g /5pσ _u
8	169.8	IP _{3/2}	
	170.8		4dδ _g
	171.0		IP _{1/2}

^a All energies were established by calibrating the S 2p_{3/2} → 3π_u^{*} transition to this value.

for the strong C 1s (2σ_g → 3π_u^{*})¹Π taken as 0.11 [9,15]. The scaling factor for the π^{*} OOS was used to derive the absolute GOS from the relative GOS for all other features. The GOS profile for the dipole-allowed C 1s(2σ_g) → 3π_u^{*} transition decreases relatively smoothly from a maximum at K² = 0. In contrast, the GOS profile for the 289.5 eV transition increases with increasing momentum transfer, consistent with its assignment as a dipole-forbidden quadrupole-allowed C 1s(2σ_g) → 3sσ_g^{*} transition. Although a quadrupole type of GOS profile was expected for the feature at 292.4 eV, since we had assigned it as the dipole forbidden C 1s(2σ_g) → 7σ_g^{*} transition [7], the experimental GOS profile clearly indicates this feature corresponds to a dipole allowed transition. The GOS profiles for the rest of the

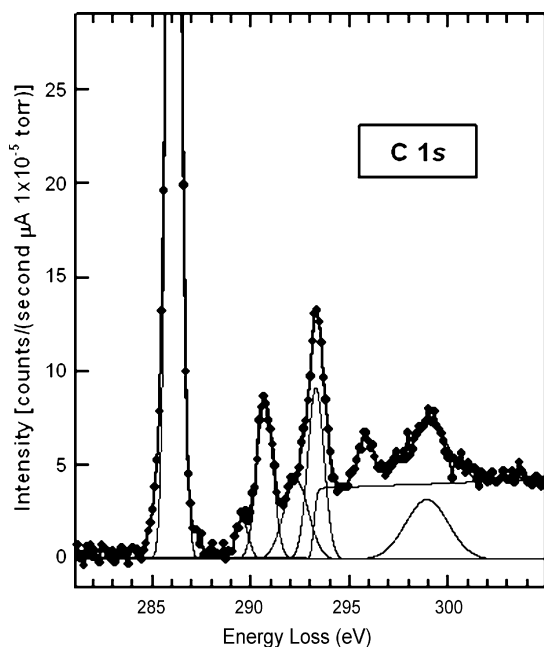


Fig. 2. Curve fits to the C 1s spectrum recorded at 4° with a final electron energy of 1300 eV, using a standardized, simultaneous multi-file curve-fit approach described in the text. The line through the data points is the result of the least squares fit, with each peak (lighter lines) represented by a Gaussian function. An error function is used to represent the C 1s continuum.

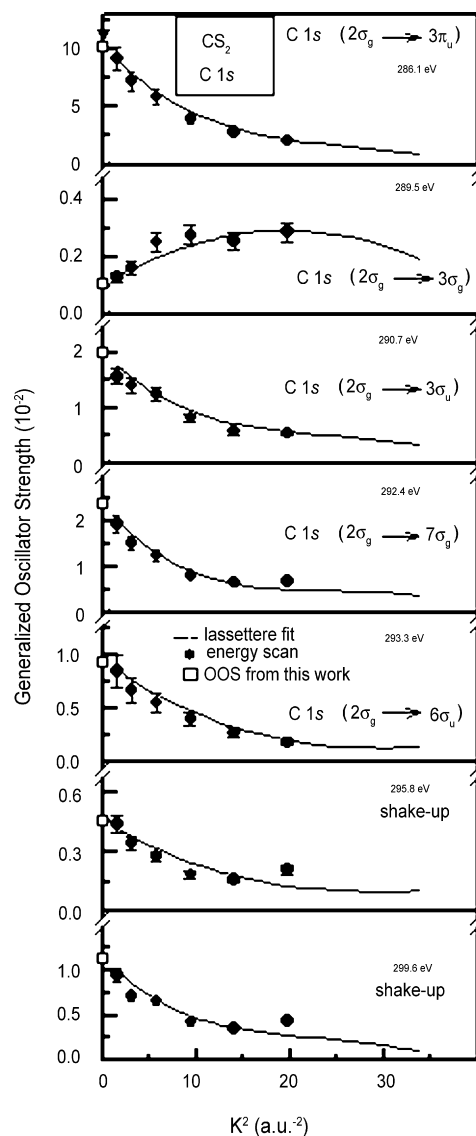


Fig. 3. Experimental GOS profiles for the C 1s transitions of CS₂ derived from EELS spectra recorded at a range of angles. The lines correspond to semi-empirical fits using Lassetre series.

resolved features smoothly decrease as K² increases, consistent with their assignments as dipole allowed transitions.

Theoretical calculations were performed for the GOS profiles for C 1s excitation to the two first π_u MOs, the two first σ_g MOs, the first σ_u and the first π_g MO. Fig. 4a compares the theoretical and experimental GOS results for the C 1s → 3π_u^{*} (286.1 eV) transition. The theoretical GOS shows the expected dipole-allowed behaviour. There is good general agreement, with the noticeable characteristic that the first Born approximation works well even for large values of K², as observed before for CO₂ [5], N₂ [13] and N₂O [16].

The measured GOS profile for the C 1s → 3sσ_g (289.5 eV) transition is compared to that computed for the C 1s → 7σ_g^{*} transition in Fig. 4b. The computed shape of the profile is that for a quadrupole-allowed transition, with zero intensity at K² = 0. However, the experimental curve shows a deviation from a smooth drop to zero towards K² = 0, which, when the data is

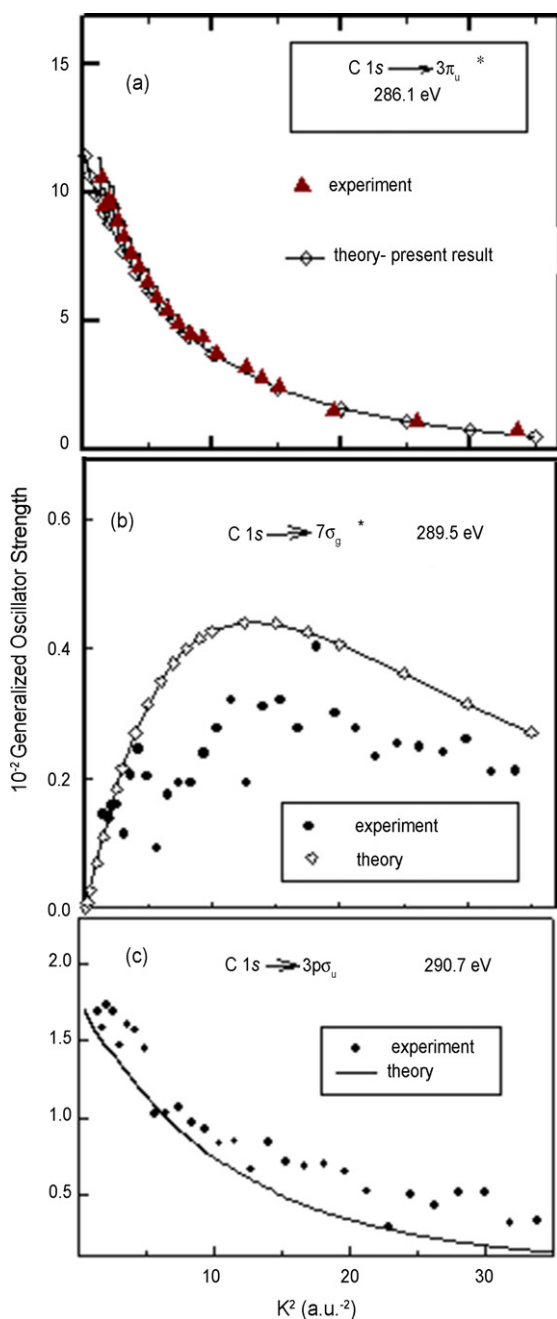


Fig. 4. (a) Theoretical and experimental GOS profiles for the $C\ 1s \rightarrow 3\pi_u^*$ transition. (b) Theoretical and experimental GOS profiles for the $C\ 1s \rightarrow 3\sigma_g/7\sigma_g^*$ transition. (c) Theoretical and experimental GOS profiles for the $C\ 1s \rightarrow 3\pi_u$ transitions.

subjected to a Lassetre fitting, indicates a finite contribution from a dipole allowed component, for example from vibronic coupling. Since the computations have not dealt with possible vibronic effects, we cannot rule out this possibility at present.

In order to compare the theoretical predictions to the measured GOS of the 290.7 eV transition, first the theoretical GOS for the excitations from $C\ 1s$ to the $6\sigma_u$ and $4\pi_u$ molecular orbitals were computed and then they were summed and compared with the experimental results, shown in Fig. 4c. There is a small vertical displacement between theoretical and experimen-

tal results. The two curves are approximately parallel and the difference between the experimental and computed optical oscillator strengths (OOS) is 0.009. This may be due to a Rydberg contribution present in the experimental results for the 290.7 eV band and not computed in the theoretical calculations.

4.3. S 2p generalized oscillator strength curves

Fig. 5 presents the GOS profiles for all resolved features in the S 2p spectrum of CS_2 . See reference [7] for spectral plots. The absolute GOS scale for the S 2p region was set by matching the graphical extrapolation to $K^2=0$ of the relative GOS profile for the $S\ 2p \rightarrow 3\pi_u^*$ feature at 163.1 eV to the optical value taken as 0.0085 [15].

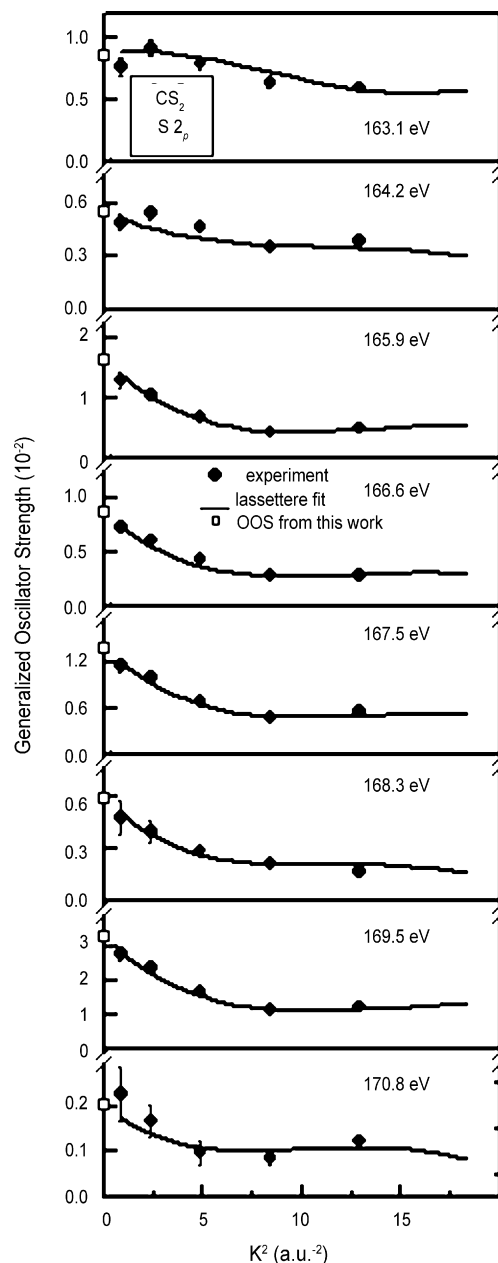


Fig. 5. GOS profiles for the S 2p transitions of CS_2 derived from EELS spectra recorded at a range of angles.

The GOS for all S 2p transitions decay relatively smoothly to higher K^2 from a maximum at $K^2 = 0$, indicating a dominant dipole-allowed process for all features. However, the decay is less for the first two curves, which in fact show a maximum around 4 a.u.^{-2} . This is an indication that the relative intensity of the first two features increase significantly with increasing momentum transfer, suggesting there is a mixture of states, some of which may be dipole forbidden. This is not surprising as the S 2p levels in CS_2 are of π_u , π_g , σ_g symmetry and the final orbital is of π_u symmetry [7]. According to the symmetry selection rules, it is possible to have a dipole forbidden transition, which would increase its intensity at higher momentum transfer.

The theoretical analysis of the S 2p excitations was performed only for states expected to contribute to the first and second, low-energy peaks. The Hamiltonian in the calculations does not take into account any coupling between orbital and spin angular momentum. Therefore, the GOS for all S 2p $\rightarrow 3\pi_u^*$ transitions was computed without spin-orbit coupling, and then their sum was compared to the sum of the experimental GOS for the S $2p_{1/2} \rightarrow 3\pi_u^*$ and S $2p_{3/2} \rightarrow 3\pi_u^*$ transitions. This assumes:

$$\text{GOS}(S 2p_{1/2}) + \text{GOS}(S 2p_{3/2}) \approx \sum_T \text{GOS}_T, \quad (5)$$

where the sum at the right side runs over all theoretical S 2p $\rightarrow 3\pi_u^*$ transitions.

The S 2p $\rightarrow 3\pi_u^*$ excitation is composed by a set of 12 transitions, listed in Table 3. Four of them are dipole allowed, six are quadrupole allowed, and two are octupole allowed. The GOS profiles for all twelve transitions were calculated. It is interesting to note that even the octupole-allowed ones give some contribution for GOS. The result at $K^2 \rightarrow 0$ is dominated by a strong dipole-allowed $4\sigma_g \rightarrow 3\pi_u^*$ transition (OOS = 0.011). The optical contribution of the other $1\pi_g \rightarrow 3\pi_u^*$ dipole-allowed transition (OOS = 0.0007) is much lower. The $3\sigma_u \rightarrow 3\pi_u^*$ transition gives a considerable quadrupole contribution to the GOS, but the strongest quadrupole contribution comes from the $1\pi_u \rightarrow 3\pi_u^*$ transition. The computed GOS profile for this transition has its maximum contribution for $K^2 = 0.5$ of 0.0003 a.u.^{-2} .

Fig. 6 plots a comparison of the computed and measured GOS profiles for the S 2p $\rightarrow 3\pi_u^*$ transition. The sum of all transitions produces a result that is in a general agreement with the sum of experimental S $2p_{1/2} \rightarrow 3\pi_u^*$ and S $2p_{3/2} \rightarrow 3\pi_u^*$ transitions.

Table 3

Possible transitions for one electron promotion from the S 2p molecular orbitals to x -manifold of the $3\pi_u$ molecular orbital^a

Initial MO	Final MO: $\rightarrow 3\pi_{u(x)}$	
	Final state	Selection rule
$4\sigma_g^+$	Π_u	Dipole
$3\sigma_u^+$	Π_g	Quadrupole
$1\pi_{g(x)}$	Σ_u^+	Dipole
$1\pi_{g(y)}$	Δ_u	Octupole
$1\pi_{u(x)}$	Σ_g^+	Quadrupole
$1\pi_{u(y)}$	Δ_g	Quadrupole

^a There is another equivalent set of six transitions for the y manifold.

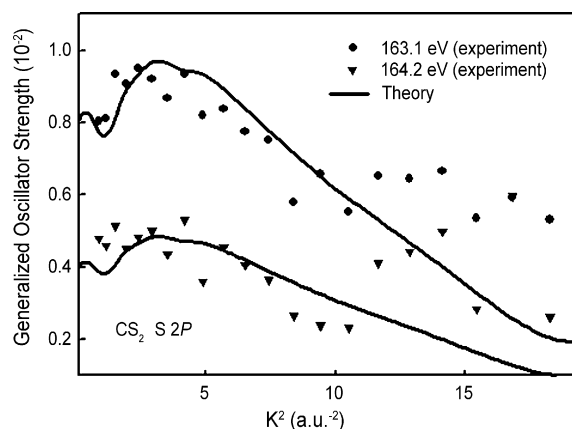


Fig. 6. Theoretical and experimental GOS profiles for the S 2p $\rightarrow 3\pi_u^*$ transitions. See text for the method used to compute the theoretical results.

In particular, both show a maximum around $K^2 = 3 \text{ a.u.}^{-2}$. The theoretical and experimental GOS diverge for large K^2 ; however this may simply reflect the large experimental uncertainties for measurements at high momentum transfer.

Although the spin-orbit coupling was not calculated, the following is a possible approach to partition the total theoretical GOS into separate $2p_{1/2}$ and $2p_{3/2}$ contributions. The simplest would be to factorize Eq. (5), by writing the GOS as

$$\text{GOS}(S 2p_{1/2}) = f \sum_T \text{GOS}_T, \quad (6a)$$

$$\text{GOS}(S 2p_{3/2}) = (1 - f) \sum_T \text{GOS}_T, \quad (6b)$$

where f is a fraction that can be determined by the OOS experimental values, or by some theoretical approach, as discussed below. f may be estimated by supposing that the transition probability for S $2p_J \rightarrow 3\pi_u^*$ excitations does not depend on the J number for high impact energy excitation, but rather is simply related to the statistical degeneracy $(2J + 1)$. Therefore, the excitation probability from the ground state would be

$$P(0 \rightarrow S 2p_J, 3\pi_u^*) \propto |\langle S 2p, 3\pi_u^* | 0 \rangle|^2 (2J + 1). \quad (7a)$$

and the ratio between GOS(S $2p_{3/2}$) and GOS(S $2p_{1/2}$) will be

$$\frac{\text{GOS}(S 2p_{3/2})}{\text{GOS}(S 2p_{1/2})} = \frac{2(3/2) + 1}{2(1/2) + 1} = 2, \quad (7b)$$

For S 2p $\rightarrow 3\pi_u^*$ excitation in CS_2 the ratio of the experimental OOS for the $2p_{3/2}$ and $2p_{1/2}$ is 1.8, possibly indicating this approach is valid, at least for CS_2 . It is important to note that there are many well known exceptions to statistical spin-orbit weights for 2p inner shell excitation of molecules containing third row elements; a particularly remarkable one occurs in PF_3 [17]. Fig. 6 presents the computed oscillator strength partitioned by the statistical weight. A relatively good agreement exists between the experimental and theoretical results suggesting the approximation used may be valid in CS_2 . However we caution that this statistical weighting partition scheme will not work for other systems such as SiF_4 (Si 2p), SF_6 (S 2p), CH_3Br (Br 3d), $\text{C}_2\text{H}_3\text{Br}$ (Br 3d), and SO_2 (S 2p) [18]. For SiF_4 for example,

the ratio of the OOS for ($\text{Si } 2p_{3/2} \rightarrow a_1^*$) and ($\text{Si } 2p_{1/2} \rightarrow a_1^*$) is 0.9:1 rather than 2. It is generally understood [17,18] that it is the exchange interaction between the core and valence electrons that is spin dependent and which modifies the intensity ratio from that expected on simple statistical degeneracy grounds. The reasonable fit in CS_2 ($2p_{3/2}:2p_{1/2}$ ratio of 1.8) may indicate the $3\pi_u^*$ orbital does not penetrate much in the S 2p region, so that the exchange interactions have relatively weak effects on the transition intensities.

5. Summary

Electron energy loss spectra of CS_2 have been recorded under dipole and non-dipole conditions in the region of S 2p, and C 1s excitation. For the first time absolute experimental GOS profiles have been derived for all resolved C 1s and S 2p features in CS_2 over an extended range of momentum transfer.

Acknowledgements

This research is supported financially by NSERC (Canada), the Canada Research Chair program, FAPERJ, and FUJB (Brazil).

References

- [1] E.N. Lassette, A. Skerbele, *Meth. Exp. Phys.* B 3 (1974) 868.
- [2] S. Trajmar, J.K. Rice, A. Kuppermann, in: L. Prigogine, S.A. Rice (Eds.), *Adv. Chem. Phys.*, vol. XVIII, Wiley, NY, 1970, p. 15;
- R.A. Bonham, in: C.R. Brundle, A.D. Baker (Eds.), *Electron Spectroscopy: Theory, Techniques and Applications*, vol. 3, Academic, NY, 1979, p. 127.
- [3] H. Bethe, *Ann. Phys. (Leipzig)* 5 (1930) 325.
- [4] M. Inokuti, *Rev. Mod. Phys.* 43 (1971) 297.
- [5] I.G. Eustatiu, T. Tylliszczak, A.P. Hitchcock, C.C. Turci, A.B. Rocha, C.E. Bielschowsky, *Phys. Rev. A* 61 (2000) 042505.
- [6] I.G. Eustatiu, J.T. Francis, T. Tylliszczak, C.C. Turci, A.L.D. Kilcoyne, A.P. Hitchcock, *Chem. Phys.* 257 (2000) 235.
- [7] I.G. Eustatiu, T. Tylliszczak, G. Cooper, A.P. Hitchcock, C.C. Turci, A.B. Rocha, M. Barbatti, C.E. Bielschowsky, *J. Electr. Spect. Rel. Phen.* (2007), doi:10.1016/j.elspec.2006.12.065, in press.
- [8] G.R. Wright, C.E. Brion, *J. Electr. Spect. Rel. Phen.* 4 (1974) 335.
- [9] A.P. Hitchcock, D.C. Mancini, *J. Electr. Spect. Rel. Phen.* 67 (1994) 1, Updates and a database of gas phase absolute results, including that for CS_2 is available from <http://unicorn.mcmaster.ca/corex.html>.
- [10] G.G.B. de Souza, M.L.M. Rocco, H.M. Boechat-Roberly, C.A. Lucas, I. Borges Jr., E. Hollauer, *J. Phys. B: At. Mol. Opt. Phys.* 34 (2001) 1005.
- [11] M.P. de Miranda, C.E. Bielschowsky, *J. Mol. Struct. (Theochem)* 282 (1993) 71.
- [12] R.E. Farren, J.A. Sheehey, P.W. Langhoff, *Chem. Phys. Lett.* 177 (1991) 307.
- [13] C.E. Bielschowsky, M.A.C. Nascimento, E. Hollauer, *Phys. Rev. A* 45 (1992) 7942.
- [14] I. Harrison, G.C. King, *J. Electr. Spect. Rel. Phen.* 43 (1987) 155.
- [15] P. Millie, A.P. Hitchcock, S. Bodeur, I. Nenner, unpublished.
- [16] C.E. Bielschowsky, M. Barbatti, A.B. Rocha, *Chem. Phys.* 299 (2004) 83.
- [17] N. Kosugi, R.G. Cavell, A.P. Hitchcock, *Chem. Phys. Lett.* 265 (1997) 490.
- [18] K.H. Sze, C.E. Brion, *Chem. Phys.* 140 (1990) 439.
- [19] C.J. Allan, U. Gelius, D.A. Allison, G. Johansson, H. Siegbahn, K. Siegbahn, *J. Electr. Spect. Rel. Phen.* 1 (1972/1973) 131.